# Optically probed symmetry breaking in the chiral magnet $Cu_2OSeO_3$

R. B. Versteeg,[1] I. Vergara,[1] S. D. Schäfer,[1] D. Bischoff,[1] A. Aqeel,[2] T. T. M. Palstra,[2]
M. Grüninger,[1] and P. H. M. van Loosdrecht[1,*]

[1]*II. Physikalisches Institut, Universität zu Köln, Zülpicher Straße 77, D-50937 Köln, Germany*

[2]*Zernike Institute for Advanced Materials, University of Groningen, Nijenborgh 4, 9747 AG Groningen, The Netherlands*

(Received 4 May 2016; published 8 September 2016)

We report on the linear optical properties of the chiral magnet $Cu_2OSeO_3$, specifically associated with the absence of inversion symmetry, the chiral crystallographic structure, and magnetic order. Through spectroscopic ellipsometry, we observe local crystal-field excitations below the charge-transfer gap. These crystal-field excitations are optically allowed due to the lack of inversion symmetry at the Cu sites. Optical polarization rotation measurements were used to study the structural chirality and magnetic order. The temperature dependence of the natural optical rotation, originating in the chiral crystal structure, provides evidence for a finite magnetoelectric effect in the helimagnetic phase. We find a large magneto-optical susceptibility on the order of $\mathcal{V}(540\ \text{nm}) \sim 10^4$ rad/T m in the helimagnetic phase and a maximum Faraday rotation of $\sim 170$ deg/mm in the ferrimagnetic phase. The large value of $\mathcal{V}$ can be explained by considering spin cluster formation and the relative ease of domain reorientation in this metamagnetic material. The magneto-optical activity allows us to map the magnetic phase diagram, including the skyrmion lattice phase. In addition to this, we probe and discuss the nature of the various magnetic phase transitions in $Cu_2OSeO_3$.

DOI: 10.1103/PhysRevB.94.094409

## I. INTRODUCTION

Materials with low symmetry exhibit a large variety of intriguing optical phenomena. As is well known, the absence of inversion symmetry leads to the occurrence of natural optical activity. In addition to this, inversion symmetry breaking strongly affects the electric dipole selection rule, and thus allows for direct excitation of local crystal-field excitations in linear spectroscopy. In magnetic materials, the breaking of time-reversal symmetry leads to the magneto-optical Kerr and Faraday effect. Many of the optical phenomena originating from a reduced symmetry have technological applications, examples of which include optical insulators and magneto-optical storage devices [1].

In recent years, materials lacking both spatial inversion and time-reversal symmetry have been a focal point of condensed matter research. Their combined absence may, for instance, lead to magneto-electric and multiferroic behavior [2–4], the formation of chiral and skyrmion magnetic ground states [5], and the occurrence of toroidal order [6,7] and excitations [8,9]. Effects on the optical properties have been studied extensively [10–12]. One intriguing optical phenomenon originating from the combined absence of time-reversal and space-inversion symmetry is the so-called nonreciprocal directional dichroism [13–16].

The high sensitivity of optical properties to symmetry breaking may be used to gain a better understanding of the underlying material properties. Here we focus on the cuprate material $Cu_2OSeO_3$, belonging to the class of noncentrosymmetric cubic crystal structures. These materials have recently triggered a great deal of research interest owing to the occurrence of topologically protected spin-vortex-like structures, known as skyrmions [5].

In these chiral crystal structures, the absence of inversion symmetry between the spin sites leads to a nonvanishing antisymmetric Dzyaloshinskii-Moriya (DM) exchange interaction, which competes with the energetically stronger isotropic Heisenberg exchange. This combination of exchange interactions stabilizes spin helices [17]. In the presence of an external magnetic field, the Zeeman interaction energy stabilizes the formation of a topologically robust hexagonal lattice of nanometer-sized skyrmions [18].

In this paper we report on a variety of linear optical properties [19] associated with the broken inversion symmetry, structural chirality, and magnetic order in the chiral magnet $Cu_2OSeO_3$ [20]. The orbital aspect of $Cu_2OSeO_3$ has only received minimal experimental attention so far [21]. Here, we reveal local crystal-field excitations below the charge-transfer gap by means of spectroscopic ellipsometry. These orbital excitations acquire a finite dipole matrix element due to the low crystal-field symmetry. Optical polarization rotation measurements are used to study the structural chirality and to probe the magnetic order. The natural optical activity, resulting from the chiral crystal structure, shows an abrupt change upon magnetic ordering. This observation is evidence of a finite magnetoelectric coupling in the phase with helical magnetic order. The large magneto-optical response is quantified by a magneto-optical susceptibility on the order of $\mathcal{V}(540\ \text{nm}) \sim 10^4$ rad/T m in the helimagnetic phase, and maximum Faraday rotation of $\sim 170$ deg/mm in the field-polarized ferrimagnetic phase. This strong response serves as an excellent probe for the various magnetic phase transitions. The magneto-optical data allow us to derive the phase diagram of $Cu_2OSeO_3$ as a function of magnetic field and temperature. The optically determined phase diagram is in excellent agreement with results obtained by other techniques [20,22,23].

## II. STRUCTURE AND MAGNETISM

$Cu_2OSeO_3$ has a complex chiral crystal structure with cubic space group $P2_13$. The unit cell contains 16 Cu ions, all having a 2+ valence state ($d^9$ configuration). These Cu ions are

*Corresponding author: pvl@ph2.uni-koeln.de

 

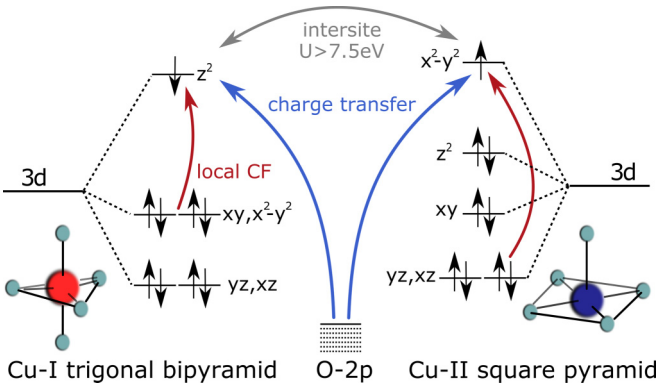


FIG. 1. The 3*d* crystal-field splittings for the Cu-I (trigonal bipyramid) and Cu-II (square pyramid) ions. The dipole-active local crystal-field (CF) excitations are indicated with red arrows, and the charge-transfer excitations with blue arrows. Intersite excitations between the Cu ions, illustrated with a gray arrow, lie outside the experimentally accessible energy range of this work.

located within two crystallographically distinct oxygen ligand field geometries [24], which can be approximated by a trigonal bipyramid ($D_{3h}$) for Cu-I ions and by a square pyramid ($C_{4v}$) for Cu-II ions, as depicted in Fig. 1. The true site symmetries are lower, and are given by $C_{3v}$ for Cu-I and $C_1$ for the Cu-II ions [24]. These ligand fields lead to different crystal-field splittings of the 3*d* orbitals on the Cu-I and Cu-II sites, as shown in Fig. 1. For Cu-I the hole is located in the $z^2$ orbital, whereas for Cu-II the hole is in the $x^2$-$y^2$ orbital. Note that these are not pure 3*d* orbitals due to the low site symmetry, i.e., parity is not a good quantum number.

The 16 Cu ions in the unit cell are distributed over four Cu-I sites and 12 Cu-II sites and form a network of corner-sharing tetrahedra, where each Cu tetrahedron comprises one Cu-I and three Cu-II ions. Owing to the different bond lengths between the 16 $Cu^{2+}$ sites in the unit cell, it is possible to make a real-space classification of the exchange energy scales into a "strong" and "weak" type [25]. Through the strong Heisenberg and DM exchange interactions, tetrahedral three-spin-up-one-down triplet clusters couple far above [25] the macroscopic ordering temperature $T_C \approx 58$ K. These $S = 1$ spin clusters turn out to be the relevant low-energy spin entities in $Cu_2OSeO_3$. The weaker intertetrahedral Heisenberg and DM exchange couplings mediate the interactions between the $S = 1$ entities, giving rise to long-range helimagnetic order below $T_C$. This separation into inter- and intratetrahedral energy scales is well supported by the splitting of the magnon spectra in two well separated energy bands [26]. Finally, weak cubic magnetic anisotropy terms pin the helimagnetic spirals along the six equivalent crystallographic ⟨100⟩ directions, leading to domain formation [22,27,28]. In the presence of an external magnetic field, different metamagnetic phases are formed. Applied magnetic fields of a few tenths of mT are enough to fully lift the degeneracy of the helical domains, giving a conical type of order with the propagation vector $q$ along the applied field. Above a second critical field the system is driven into the field-polarized ferrimagnetic phase, where all tetrahedral $S = 1$ entities are aligned with the magnetic field. The skyrmion lattice phase (SkL) is located within a narrow field-temperature window just below $T_C \approx 58$ K for moderate applied fields of the order of 20–50 mT [20,22].

## III. EXPERIMENTAL METHODS

High-quality single crystals were grown using a standard chemical vapor transport method [29]. Single crystal x-ray diffraction [30] measurements and our optical polarization rotation measurements show that $Cu_2OSeO_3$ single crystals are chiral, and that both handednesses can be realized experimentally. The studied crystals were oriented by crystal morphology inspection after which the fine orientation was done by means of a Laue camera. For the ellipsometry study a (100) surface was prepared (sample surface dimensions approximately 2.7 mm × 2.8 mm, thickness 0.8 mm). For the polarimetry study, two (111) oriented samples with opposite crystallographic chirality were used. A levorotatory crystal (as seen from the source) was chosen for the temperature- and field-dependent polarization rotation measurements. The surface area was approximately 3.6 mm × 3.2 mm, with used thicknesses of $d \approx 1.00$ mm and $d \approx 221 \pm 3$ $\mu$m. The dextrorotatory crystal, used for a consistency check of the natural optical activity, had a surface area of approximately 2.1 mm × 1.8 mm and thickness $d \approx 223 \pm 3$ $\mu$m. All samples were polished with $Al_2O_3$ suspension ($\approx 1$ $\mu$m grain size) in order to obtain optically smooth surfaces.

For the optical spectroscopy part, a Woollam VASE spectroscopic ellipsometer with an autoretarder between source and sample was used. Ellipsometry allows us to obtain the real and imaginary parts of the complex dielectric function in a self-normalizing way. The (100) sample was mounted in a UHV chamber with a liquid-He flow cryostat and measured in the range 0.75–5 eV at a fixed angle of incidence (70°). For the analysis of the ellipsometric data, the surface roughness was estimated using the knowledge that absorption is small in the transparency windows below 1 eV and around 2.3 eV.

For the polarization rotation measurements we used a homebuilt optical polarimetry setup based on the polarization modulation technique described in Refs. [31,32]. Measurements are possible in the energy range of 1.1–3.5 eV in fields up to 5 T and temperatures down to 10 K. The measurements are performed in Faraday (transmission) geometry, where the light propagates along the crystallographic [111] direction, with the magnetic field also applied along this direction.

## IV. ZERO-FIELD OPTICAL PROPERTIES

### A. Optical excitations

In Fig. 2 the diagonal component $\sigma_{xx,1}$ of the optical conductivity at 15 and 300 K is shown. We find a clear electronic gap with an onset at about 2.5 eV at 15 K, and charge-transfer excitations peaking at 3.2 and 4.0 eV with an optical conductivity of about 400 and 1200 $\Omega^{-1}\,\mathrm{cm}^{-1}$, respectively. Hubbard-augmented density functional theory (DFT+$U$) calculations find narrow Cu hole bands for both Cu sites with an energy difference of about $\Delta E = E_{\mathrm{II}} - E_{\mathrm{I}} = 0.2$ eV, while the valence band primarily consists of broad oxygen bands [33]. Based on this, we tentatively attribute the structure in the charge-transfer region to both the splitting $\Delta E$ and the structure in the O 2$p$ valence band density of states.

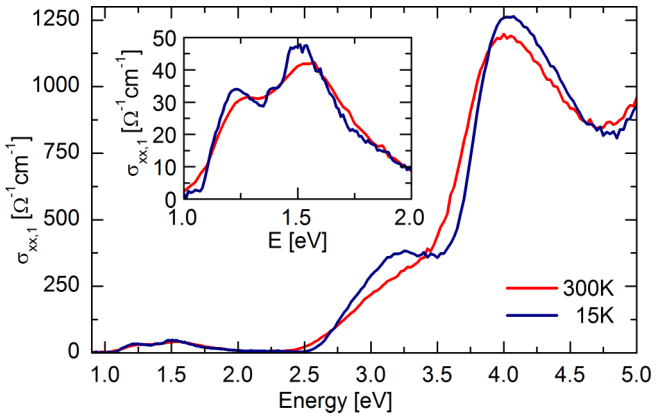


FIG. 2. Optical conductivity at 15 and 300 K as obtained by ellipsometry. The onset of charge-transfer excitations is observed at about 2.5 eV at 15 K. Between 1.0 and 2.0 eV local crystal-field excitations are observed with conductivity values not surpassing 50 $\Omega^{-1}$ cm$^{-1}$. At 15 K, pronounced peaks are located at 1.2, 1.4, and 1.5 eV. The features broaden with increasing temperature, obscuring the 1.4 eV peak at 300 K, as seen in the inset.

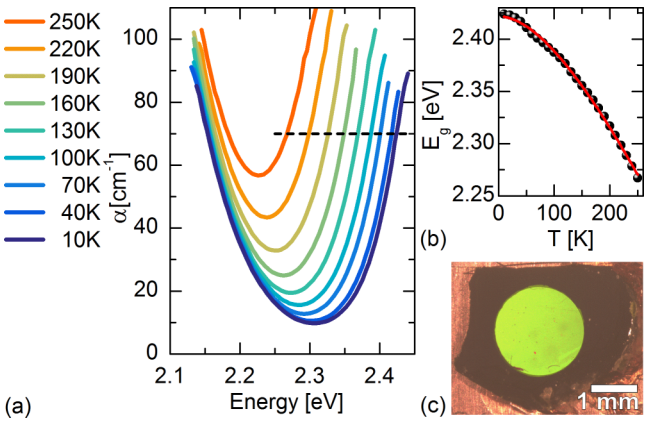


FIG. 3. (a) Temperature-dependent absorption spectra in the range of the transmission window as measured on the 1-mm-thick sample. (b) Temperature dependence of the onset $E_g$ of excitations across the gap, determined at $\alpha = 70$ cm$^{-1}$. The fit (red line) is based on the empirical Varshni equation. (c) $Cu_2OSeO_3$ is transparent for green light. The (111) sample, with a thickness $d \approx 221 \pm 3$ $\mu$m, is glued on a copper sample holder with a 2.0-mm-diameter hole.

With decreasing temperature, the charge-transfer excitations show a blueshift and a sharpening.

The first consequence of the low structural symmetry appears in the optical conductivity. Between 1.0 and 2.0 eV we find a multipeak absorption feature, with a conductivity maximum of about 50 $\Omega^{-1}$ cm$^{-1}$, i.e., much weaker than the charge-transfer excitations (see inset of Fig. 2). At 15 K, pronounced peaks are located at 1.2, 1.4, and 1.5 eV. The peaks broaden with increasing temperature, obscuring the peak at 1.4 eV at 300 K. We interpret these features as local crystal-field (CF) excitations. Similar excitation energies were observed before for CF excitations of $Cu^{2+}$ ions in a trigonal bipyramidal crystal field [34]. For materials with inversion symmetry at the transition-metal site, such crystal-field excitations would be parity forbidden within the dipole approximation. They only become weakly allowed via the simultaneous excitation of an inversion-symmetry-breaking odd-parity phonon. Typical values of $\sigma_1(\omega)$ for such phonon-assisted excitations are below 10 $\Omega^{-1}$ cm$^{-1}$ [35]. In contrast, the absence of inversion symmetry at the Cu-I and Cu-II sites in $Cu_2OSeO_3$ allows for dipole-active CF excitations by symmetry, and thus naturally explains the sizable spectral weight below the gap between 1.0 and 2.0 eV.

According to group theory [36], dipole-active excitations are allowed from $xy$ and $x^2$-$y^2$ to $z^2$ for the Cu-I site (assuming $D_{3h}$ symmetry) and from $xz$ and $yz$ to $x^2$-$y^2$ for the Cu-II site (assuming $C_{4v}$ symmetry). Both sets of transitions are schematically indicated in Fig. 1. The spectral weight in the low-energy region, however, has a richer structure with at least three peaks at 15 K. In the above-mentioned analysis we ignored the fact that the Cu sites show a slight distortion away from the ideal square pyramidal and trigonal bipyramidal symmetries. Considering the correct, lower site symmetries, the remaining crystal-field excitations also are dipole active and will also contribute to the total spectral weight. Note that the two peak energies observed at 300 K *soften* to lower energy with decreasing temperature (see the Appendix for a more detailed $T$ dependence). This is opposite to the behavior of the charge-transfer peaks and can be attributed to the asymmetric line shape found, in particular, at low temperature. Such an asymmetric line shape can be described by the Franck-Condon line shape typical for crystal-field excitations [35,37].

Our assignment of the onset of charge-transfer excitations to an energy of about 2.5 eV is corroborated by the observation of a narrow transmission window which is situated between the crystal-field excitations and the charge-transfer region. At 10 K the absorption coefficient becomes as low as 10 cm$^{-1}$ at 2.3 eV (see Fig. 3). On the low-energy side the absorption decreases with decreasing temperature due to the sharpening of the crystal-field excitations. On the high-energy side a more drastic change of the absorption coefficient is found, reflecting the temperature dependence of the onset $E_g$ of excitations across the gap. This temperature dependence is well described by the empirical Varshni equation [38], as seen in Fig. 3(b).

Previously, Miller *et al.* [39] reported on the optical conductivity of $Cu_2OSeO_3$ at 300 K based on a Kramers-Kronig analysis of reflectivity data. Above 2.5 eV, their data reasonably agree with our results, showing a dominant peak at 4 eV. However, a Kramers-Kronig analysis is not sensitive to weak absorption features, thus the crystal-field excitations between 1.0 and 2.0 eV were not resolved. Additionally, Miller *et al.* [39] reported on a transmission window in the frequency range above the phonons and below about 1 eV, which agrees with the onset of crystal-field excitations observed in our data.

### B. Natural optical activity

Due to the chiral crystal structure, $Cu_2OSeO_3$ is expected to show circular birefringence with a concomitant optical rotation for linearly polarized light, known as natural optical activity with rotation angle $\theta_{NOA}$ [19,40]. The low absorption around 2.3 eV allows us to measure the polarization rotation in transmission geometry. As a probe wavelength we used $\lambda_{probe} = 540 \pm 5$ nm ($E_{probe} = 2.30 \pm 0.03$ eV), which

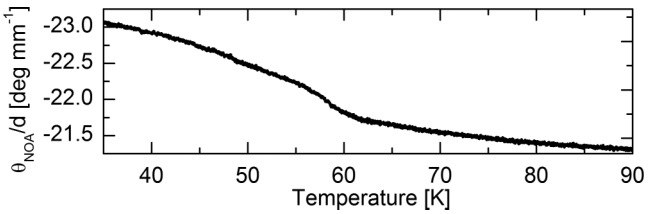


FIG. 4. The natural optical activity $\theta_{\mathrm{NOA}}$ per sample thickness $d$ in deg/mm measured along the crystallographic (111) axis with probe photon energy $E_{\mathrm{probe}} = 2.30 \pm 0.03$ eV. The crystal is levorotatory. Above the Curie temperature $T_C \approx 58$ K, the temperature dependence is weak. Below $T_C$ an enhancement of $\theta_{\mathrm{NOA}}$ is observed, which is attributed to the finite magnetoelectric coupling in the helimagnetically ordered state.

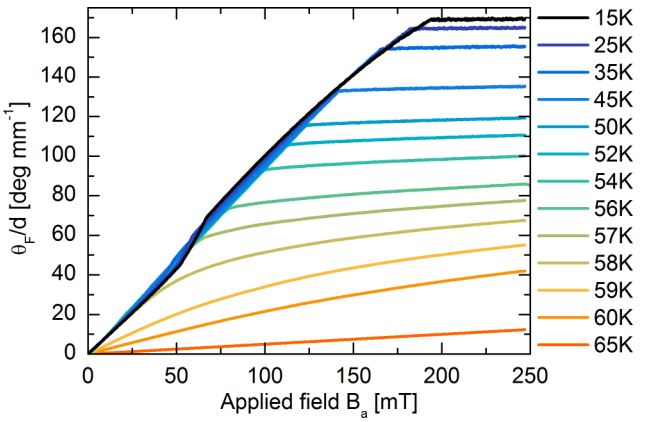


FIG. 5. The Faraday rotation per sample thickness, $\theta_{\mathrm{F}}/d$, as a function of field for different temperatures. With increasing field, $\theta_{\mathrm{F}}$ increases until a plateau is reached, marking the phase transition between conical and ferrimagnetic order. At 15 K this phase transition is induced around an applied field of $B_a \approx 195$ mT. At lower fields, in the 15 K curve around $B_a \approx 60$ mT, the helical-conical phase transition becomes apparent as a kink in the field dependence of $\theta_{\mathrm{F}}/d$.

corresponds to the transmission maximum at low temperature. At room temperature, both the left- and the right-handed (111) oriented crystals have a rotation magnitude of around 18 deg/mm, but the sign of the polarization rotation changes with crystallographic handedness. When the light propagation direction is reversed, the rotational sense remains the same for both crystals. The latter two observations are regarded as earmarks for the phenomenon of natural optical activity [41].

The temperature dependence of $\theta_{\mathrm{NOA}}$ across the paramagnetic-helimagnetic phase transition ($T_C \approx 58$ K) was measured for the levorotatory crystal. The result is given in Fig. 4, showing $\theta_{\mathrm{NOA}}/d$. Above $T_C$ a finite $\theta_{\mathrm{NOA}}/d$ of around $-21.5$ deg/mm is found. The temperature dependence of $\theta_{\mathrm{NOA}}$ in the paramagnetic phase hints at an increase of the structural chirality upon lowering temperature, i.e., a displacement of ions at general coordinates within the $Cu_2OSeO_3$ unit cell, satisfying the threefold rotational symmetry of the structural helix.

In the helimagnetically ordered phase, the temperature dependence of $\theta_{\mathrm{NOA}}$ is enhanced. Since there is no net magnetization in the helimagnetic phase for $B_a = 0$ mT [27] no Faraday rotation is expected. Different studies suggest that no significant magnetostrictive lattice contraction nor lattice deformations are present in $Cu_2OSeO_3$ related to the transition into the helimagnetic phase [24,42]. Instead, the increasing $\theta_{\mathrm{NOA}}$ strongly hints to the presence of a finite magnetoelectric coupling in the helimagnetic phase, as suggested in Refs. [23,24,27,28].

## V. MAGNETO-OPTICAL PROPERTIES

### A. Phase transitions

In the presence of a magnetic field $B_a \parallel [111]$, different metamagnetic phases with a finite magnetization $M(B_a)$ form in $Cu_2OSeO_3$ [20]. For these phases, the total polarization rotation can be approximated by

$$\theta_{\mathrm{tot}} \approx \theta_{\mathrm{NOA}} + \theta_{\mathrm{F}}[M(B_a)], \tag{1}$$

where $\theta_{\mathrm{F}}$ denotes the Faraday rotation which is proportional to the magnetization $M(B_a)$ in the [111] direction [43]. The field-dependent magnetization can be rewritten as $M(B_a) = \chi_m(B_a)B_a$, where $\chi_m(B_a)$ refers to the magnetic susceptibility. Note that the magnetic susceptibility $\chi_m$ itself is a function of the external field. We thus probe a Faraday rotation per sample thickness $d$ of

$$\begin{aligned} \frac{1}{d}\theta_{\mathrm{F}}[\omega, M(B_a)] &= \beta(\omega)M(B_a), \\ &= \beta(\omega)\chi_m(B_a)B_a, \end{aligned} \tag{2}$$

where $\beta(\omega)$ captures the microscopic magneto-optical properties.

Figure 5 shows the Faraday rotation per sample thickness, $\theta_{\mathrm{F}}/d$, as a function of field $B_a$ for temperatures ranging from 15 to 65 K. At zero applied field, different helimagnetic domains exist. However, there is no net magnetization, even for a single helical domain. In this way, $\theta_{\mathrm{F}}$ is zero for $B_a = 0$ mT [27]. With increasing field the helimagnetic domains acquire a conical contribution, leading to a finite field-induced magnetization $M(B_a)$, and hence a Faraday rotation. The multi-$q$ helimagnetic domain structure, however, still persists. At a critical field of around 60 mT at 15 K, the reorientation transition from the multi-$q$ helical to the single-$q$ conical phase is observed. With increasing field, the spin projection parallel to $q$ and $B_a$ increases. It is for this reason that in the conical phase the Faraday rotation still increases with field, until a plateau is reached, marking the phase transition from conical to field-polarized ferrimagnetic order. At 15 K this phase transition is induced around an applied field of $B_a \approx 195$ mT. At the plateau a rotation of around 170 deg/mm is found for 15 K. The Faraday rotation sense was determined to be positive [44].

The second derivative [45] of the Faraday rotation allows us to construct the phase diagram shown in Fig. 6. The right panel gives a zoom-in around $T_C$. In this way the phase transitions to the SkL phase become apparent. With a field applied along the ⟨111⟩ hard axis, the phase transition from conical to ferrimagnetic order (indicated by triangles) is of second order [25], and the phase transition can be identified with a

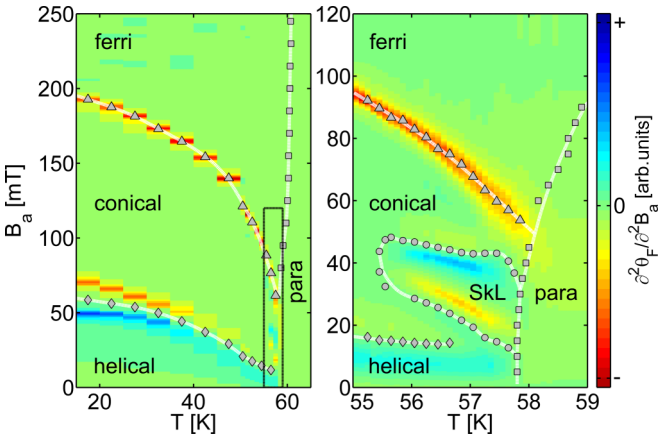


FIG. 6. The magnetic phase diagram of $Cu_2OSeO_3$ as obtained from the Faraday rotation. $B_a$ is the applied magnetic field along the crystallographic (111) direction. The left panel shows the magnetic phase diagram for a large $(B_a, T)$ range, whereas the right panel gives a zoom-in around the skyrmion lattice phase (SkL). The triangles indicate the conical-ferrimagnetic phase boundary. Diamonds give the helical-conical phase boundary. The SkL phase boundary is indicated by the circles. The phase boundary between ordered phases and the paramagnetic phase is indicated by the squares. The color mapping indicates the second derivative of the Faraday rotation. For a quantitative comparison of the critical fields with results obtained by other techniques, one needs to take into account the demagnetization factor (see main text).

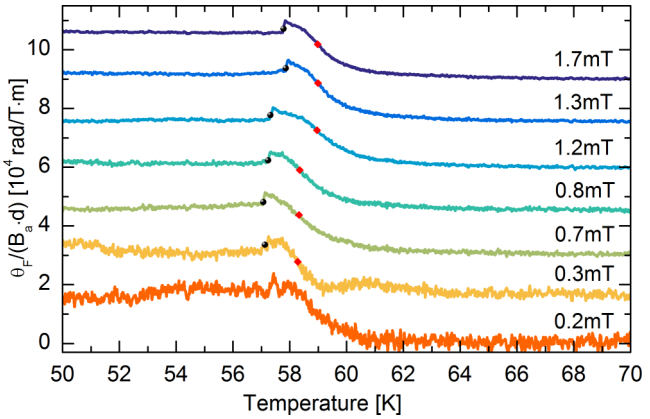


FIG. 7. Faraday rotation across the paramagnetic-helimagnetic phase transition, normalized by applied field $B_a$. The curves are offset by $(\pi/1.8) \times 10^4$ rad/T m with respect to each other. Within the helical phase the scaled rotation attains a value of $\theta_F/(B_a d) \approx 1.7 \times 10^4$ rad/T m. The weak first-order transition into the helical phase is marked by black circles. The fluctuation-disorder regime is located between the black dot and the red diamond.

local minimum in the second derivative of the order parameter $M \propto \theta_F$. The phase transitions from helical to conical order (diamonds) and between the conical phase and the SkL phase (indicated by circles) are of first order and can be identified with a zero crossing in the second derivative of $\theta_F$. The diamonds and circles in Fig. 6 indicate these zero crossings, marking the phase boundaries.

The phase transitions from the paramagnetic phase to the ordered phases are best observed in temperature sweeps at constant field. Depending on the field strength, different phase transitions occur. Figure 7 shows $\theta_F/(B_a d)$ across the paramagnetic-helimagnetic phase transition for $|B_a| < 2$ mT. At low temperatures, deep within the helimagnetic phase, $\theta_F/(B_a d)$ does not show a significant temperature dependence. However, an anomaly is observed around the paramagnetic-helimagnetic transition. In fact, the anomaly marks $T_C$. In mean-field approximation this phase transition is expected to be of second order. However, the interaction between chiral fluctuations renormalizes the phase transition into a weak first-order transition [46], as seen in the temperature dependence of $\theta_F/(B_a d)$. Just above the phase transition, we find the fluctuation-disordered region [47] where the magnetic susceptibility deviates from pure Curie-Weiss behavior. The onset of this region is identified by the inflection point, located about 1 K above $T_C$ (indicated by the red diamonds).

The high-field phase transitions from the paramagnetic to the ordered phases are best seen in the temperature dependence of the first derivative $d\theta_F/dB_a$, at different values of $B_a$. Here, we define the first derivative as a magneto-optical susceptibility

$$\chi_{MO} = \frac{1}{d}\frac{d\theta_F}{dB_a} = \beta(\omega)\left[\chi_m(B_a) + \frac{\partial \chi_m}{\partial B_a} B_a\right], \qquad (3)$$

as shown in Fig. 8. The temperature and field dependence of $\chi_{MO}$ show reasonable agreement with the magnetic ac susceptibility as reported by Živković *et al.* [48] Small deviations can be attributed to the field dependence of $\chi_m$.

For 5 mT the characteristic anomaly for the paramagnetic-helimagnetic transition is visible again. For applied fields of 15, 25, and 45 mT the first-order nature remains for the paramagnetic-SkL and paramagnetic-conical transitions. The broad maximum found at lower temperatures for these applied fields indicates the temperature-induced conical-helical phase

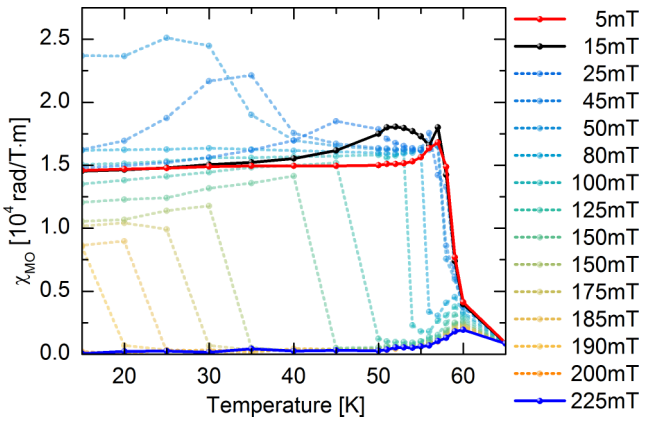


FIG. 8. The magneto-optical susceptibility $\chi_{MO}$ as a function of temperature at different applied field strengths. The phase transition from the paramagnetic phase to one of the ordered phases shows a rescaling from first order (for the para to helical/conical/SkL phases) to second order (para-ferri) with increasing field. The changes in $\chi_{MO}$ below $T_C \approx 58$ K show the temperature-induced conical-helical and ferrimagnetic-conical phase transitions.

transition. At higher fields such as 100, 150, and 225 mT, the paramagnetic-ferrimagnetic phase transition is crossed. The magneto-optical susceptibility for these field values shows that the character of the phase transition changes to second order. For $Cu_2OSeO_3$, this change of the phase-transition type has been discussed extensively by Živković *et al.* [48]. The increase in $\chi_{MO}$ at lower temperatures for field values between 80 and 190 mT shows where the temperature-induced ferrimagnetic-conical phase transition is crossed. With the first derivative, the phase diagram can be completed. The boundary between the paramagnetic phase and the ordered phases is indicated by squares in the phase diagram.

Qualitatively, the phase diagram that we have determined by optical means is in excellent agreement with previously reported results based on other techniques [20,22,23]. For a quantitative comparison of the applied field strengths at which the phase transitions are observed, one has to take into account demagnetization effects related to the sample shape. For the optical measurements in transmission geometry, we used a thin plate for which demagnetization effects are substantial. The demagnetization factor can be estimated [49] to lie around $N_z \approx 0.9$. Accordingly, the phase transitions occur at higher applied fields than, for instance, in a spherical sample with $N_z = 1/3$.

### B. Field-even rotation and directional dichroism

Phenomenologically, the measured polarization rotation $\theta_{tot}(B_a)$ can be split into odd and even contributions, $\theta_{odd/even}(B_a) = [\theta_{tot}(+B_a) \mp \theta_{tot}(-B_a)]/2$. In systems which simultaneously lack time-reversal and spatial inversion symmetry, one may expect a field-even contribution to the Faraday effect, in addition to the usual field-odd effect [1,50,51].

We indeed find a finite polarization rotation even in $B_a$, as shown in Fig. 9. Besides the Faraday rotation, the natural optical activity of chiral magnets lacking spatial inversion symmetry may show a field-even variation as well [52,53]. Unfortunately, the present experiments do not allow us to discriminate between these contributions. At 15 K, $\theta_{even}$ constitutes less than about 2% of the measured field-dependent polarization rotation. With increasing field, $\theta_{even}$ increases until the ferrimagnetic phase is reached, where the rotation levels off. At the helical-conical phase transition, a jagged feature appears. This feature reflects hysteretic behavior. Since the sweeps were performed between opposite field polarities, the phase transitions are traversed in opposite direction, i.e., the applied field either decreases or increases. Symmetrization of the hysteretic behavior leads to the jagged feature. Such hysteretic behavior in the field direction has also been observed for phase transitions in other cubic chiral magnets, as for instance in $Fe_{1-x}Co_xSi$ [54].

The magnetic chiral structure allows for an additional higher-order optical effect, namely, nonreciprocal directional dichroism [13,14]. In $Cu_2OSeO_3$ this effect has been observed for microwave resonance modes [55]. We have investigated this effect in the optical range (around 2.3 eV) for the various magnetic phases at 15 K, but have not been able to make a conclusive observation. Given the sensitivity of our setup, this limits a possible nonreciprocal directional dichroism to well below 1%.

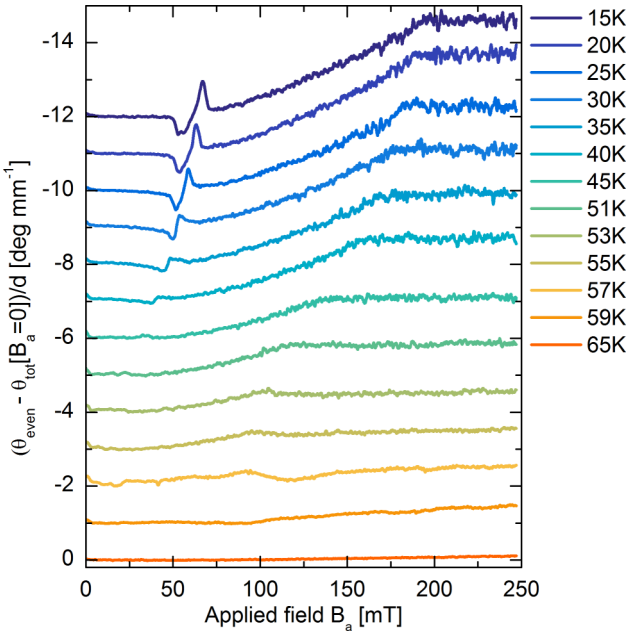


FIG. 9. The field-even rotation $\theta_{even}$, shown here per sample thickness $d$ for some selected temperatures. The curves are offset by $-1$ deg/mm for clarity. The phase transition from conical to ferrimagnetic order again becomes apparent. The jagged feature at the helical-conical phase transition is due to hysteresis in $\theta_F$.

### C. Magnitude of the magneto-optical effect

At 15 K, we find a polarization rotation of around 170 deg/mm in the field-polarized ferrimagnetic phase above 195 mT and a magneto-optical susceptibility of the order of $10^4$ rad/T m for smaller magnetic fields. In the following, we will show that both values are large but can be explained by the fact that the spin clusters are fully polarized already for moderate magnetic fields of 195 mT.

For a field-independent magnetic susceptibility, the size of the magneto-optical response can be expressed by the Verdet coefficient $\mathcal{V}(\omega) = \beta(\omega)\chi_m$ [cf. Eq. (3)]. In the helical phase at low temperatures and small fields the field dependence of $\chi_m$ is only small. This is apparent from the magneto-optical susceptibility $\chi_{MO}$ (see Fig. 8). To first approximation we therefore assign a Verdet coefficient of $1.5 \times 10^4$ rad/T m in the helical phase. Taking into account the demagnetizing field correction [48,49], we find $\mathcal{V}(540\ \text{nm}) \approx 3 \times 10^4$ rad/T m, a value rivaling known strong magneto-optical rotators such as the paramagnets $Tb_3Ga_5O_{12}$ (with $\mathcal{V}(1053\ \text{nm}) \approx 0.3 \times 10^4$ rad/T m at 4.2 K) [56] and $Cd_{1-x}Mn_xTe$ ($\mathcal{V} \lesssim 9 \times 10^4$ rad/T m at 77 K depending on $\omega$ and stoichiometry) [57]. For these paramagnets, the large size of $\mathcal{V}$ solely originates in $\beta(\omega)$ [43]. In contrast, the large magneto-optical response of $Cu_2OSeO_3$ can be attributed to the large magnetic susceptibility at low fields and the strong magnetization at larger fields.

The magnetization [24] of $Cu_2OSeO_3$ shows that the $S = 1$ clusters are fully aligned along the applied field in the ferrimagnetic phase, i.e., already for moderate magnetic fields of 0.2 T. This reflects that the magnetocrystalline anisotropy is weak in this cubic magnet with small spin-orbit coupling.

As a result, the helical or conical domains can be easily reoriented [58], even when the magnetic field is applied along the ⟨111⟩ hard axis. This in turn is reflected in a large magnetic susceptibility $\chi_m$, and hence a large magneto-optical susceptibility $\chi_{\mathrm{MO}}$.

For the field-polarized ferrimagnetic phase, strong magneto-optical effects are naturally expected. In fact, roughly similar (volume) magnetizations and polarization rotations have been observed in ferromagnetic cuprates such as the two-dimensional compounds $K_2CuF_4$ [59] and $(CH_3NH_3)_2CuCl_4$ [60], showing rotations of 36 deg/mm and 50 deg/mm, respectively. This shows that the magneto-optical coupling $\beta(\omega)$ in $Cu_2OSeO_3$ is of equal order of magnitude as in these materials.

The microscopic magneto-optical interaction $\beta(\omega)$ depends on the difference in dipole transition strength for the $\sigma_+$ and $\sigma_-$ transitions at $\omega$, where $\pm$ refers to right/left circularly polarized light, respectively [43]. A *larger* difference in transition strength leads to a *stronger* rotation. In a ferromagnet with full spin polarization, only one of the transitions $\sigma_\pm$ is preferentially allowed due to angular momentum conservation.

In contrast, a perfect antiferromagnet with zero magnetization shows equal transition strengths and thus no polarization rotation. In $Cu_2OSeO_3$, one finds a ferromagnetic alignment of the $S = 1$ clusters but antiferromagnetic alignment between Cu-I and Cu-II sites within a given cluster (see Fig. 1). However, the excitation energies are different for Cu-I and Cu-II sites, which holds for both the crystal-field excitations and charge-transfer excitations. In addition, the Cu-I and Cu-II sites are present in a ratio of 1:3. Accordingly, the cancellation typical for a simple antiferromagnet does not occur in $Cu_2OSeO_3$. Moreover, the transition dipole strength of both types of excitations is relatively large, which magnifies the magneto-optical response. Whether the different optical transitions have the same rotational sense or not cannot be answered based on a single-wavelength measurement and remains open for further studies.

## VI. CONCLUSIONS

We have shown how a variety of linear optical properties can be used to probe inversion and time-reversal breaking properties of the chiral magnetic cuprate $Cu_2OSeO_3$. The broken inversion symmetry at the two crystallographically inequivalent Cu sites leads to a finite dipole matrix element for local crystal-field excitations. These orbital excitations were observed below the charge-transfer gap, in the energy range from 1.0 to 2.0 eV. The transmission window found between the crystal-field and the charge-transfer absorption regions allowed us to measure the optical polarization rotation across the various magnetic phase transitions in $Cu_2OSeO_3$. The zero-field optical rotation, corresponding to the natural optical activity of the crystal, is enhanced upon entering the helimagnetically ordered phase. This observation provides evidence for a finite magneto-electric coupling in the helimagnetic phase of $Cu_2OSeO_3$.

In the presence of an external magnetic field, the finite magnetization leads to a sizable Faraday rotation. The ease of domain reorientation by the external magnetic field was discussed to be at the origin of the large magneto-optical susceptibility in the helical and conical phases. The large Faraday rotation observed in the field-polarized ferrimagnetic phase agrees with results obtained on ferromagnetic cuprates. The Faraday rotation provides a sensitive tool to conveniently probe the nature of the various magnetic phase transitions in $Cu_2OSeO_3$, including the subtle first-order nature of the helimagnetic-paramagnetic phase transition. From the magneto-optical data we reconstructed the phase diagram of $Cu_2OSeO_3$ as a function of magnetic field and temperature, including the skyrmion lattice phase.

## ACKNOWLEDGMENTS

The authors are grateful to M. Garst, A. Rosch, P. Becker, L. Bohatý, T. Lorenz, and G. R. Blake for insightful discussions. We also thank P. Padmanabhan for critical reading of the manuscript. Part of this work was financially supported by the Bonn-Cologne Graduate School of Physics and Astronomy (BCGS), and the Deutsche Forschungsgemeinschaft (DFG) through the Collaborative Research Center SFB 1238, projects B02 and B05.

## APPENDIX: TEMPERATURE DEPENDENCE OF ELLIPSOMETRY DATA

The temperature dependence of the optical conductivity in the region of the crystal-field excitations is shown in more detail in Fig. 10. The inset shows the temperature dependence of the spectral weight of this region, i.e., the integral of $\sigma_1(\omega)$ from 1 to 2 eV. We find a slight increase of the spectral weight with increasing temperature. The onset of magnetic order at 58 K has no significant effect on the spectral weight of the crystal-field excitations.

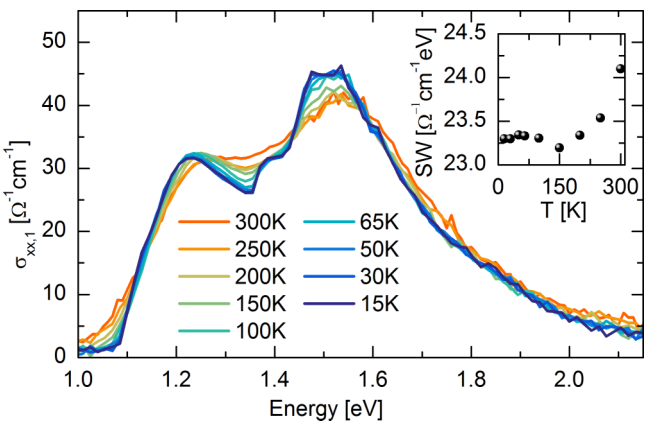


FIG. 10. Optical conductivity in the region of the crystal-field excitations for different temperatures. The inset depicts the spectral weight (integral of the optical conductivity between 1.0 and 2.0 eV) as a function of temperature.

[1] A. K. Zvezdin and V. A. Kotov, *Modern Magnetooptics and Magnetooptical Materials* (Institute of Physics Publishing, London, 1997).

[2] Y. Tokura, S. Seki, and N. Nagaosa, Multiferroics of spin origin, Rep. Prog. Phys. **77**, 076501 (2014).

[3] D. I. Khomskii, Trend: Classifying multiferroics: Mechanisms and effects, Physics **2**, 20 (2009).

[4] D. I. Khomskii, Multiferroics: Different ways to combine magnetism and ferroelectricity, J. Magn. Magn. Mater. **306**, 1 (2006).

[5] N. Nagaosa and Y. Tokura, Topological properties and dynamics of magnetic skyrmions, Nat. Nanotechnol. **8**, 899 (2013).

[6] N. A. Spaldin, M. Fiebig, and M. Mostovoy, The toroidal moment in condensed-matter physics and its relation to the magnetoelectric effect, J. Phys.: Condens. Matter **20**, 434203 (2008).

[7] A. S. Zimmermann, D. Meier, and M. Fiebig, Ferroic nature of magnetic toroidal order, Nat. Commun. **5**, 4796 (2014).

[8] T. Kaelberer, V. A. Fedotov, N. Papasimakis, D. P. Tsai, and N. I. Zheludev, Toroidal dipolar response in a metamaterial, Science **330**, 1510 (2010).

[9] N. Papasimakis, V. Fedotov, V. Savinov, T. Raybould, and N. I. Zheludev, Electromagnetic toroidal excitations in matter and free space, Nat. Mater. **15**, 263 (2016).

[10] B. B. Krichevtsov, V. V. Pavlov, R. V. Pisarev, and V. N. Gridnev, Spontaneous non-reciprocal reflection of light from antiferromagnetic $Cr_2O_3$, J. Phys.: Condens. Matter **5**, 8233 (1993).

[11] A. Pimenov, A. A. Mukhin, V. Yu. Ivanov, V. D. Travkin, A. M. Balbashov, and A. Loidl, Possible evidence for electromagnons in multiferroic manganites, Nat. Phys. **2**, 97 (2006).

[12] P. Rovillain, J. Liu, M. Cazayous, Y. Gallais, M.-A. Measson, H. Sakata, and A. Sacuto, Electromagnon and phonon excitations in multiferroic $TbMnO_3$, Phys. Rev. B **86**, 014437 (2012).

[13] G. L. J. A. Rikken and E. Raupach, Pure and cascaded magnetochiral anisotropy in optical absorption, Phys. Rev. E **58**, 5081 (1998).

[14] D. Szaller, S. Bordács, and I. Kézsmárki, Symmetry conditions for nonreciprocal light propagation in magnetic crystals, Phys. Rev. B **87**, 014421 (2013).

[15] I. Kézsmárki, D. Szaller, S. Bordács, V. Kocsis, Y. Tokunaga, Y. Taguchi, H. Murakawa, Y. Tokura, H. Engelkamp, T. Rõõm, and U. Nagel, One-way transparency of four-coloured spin-wave excitations in multiferroic materials, Nat. Commun. **5**, 3203 (2014).

[16] S. Toyoda, N. Abe, S. Kimura, Y. H. Matsuda, T. Nomura, A. Ikeda, S. Takeyama, and T. Arima, One-Way Transparency of Light in Multiferroic $CuB_2O_4$, Phys. Rev. Lett. **115**, 267207 (2015).

[17] P. Bak and M. H. Jensen, Theory of helical magnetic structures and phase transitions in MnSi and FeGe, J. Phys. C: Solid State Phys. **13**, L881 (1980).

[18] U. K. Rößler, A. A. Leonov, and A. N. Bogdanov, Chiral skyrmionic matter in non-centrosymmetric magnets, J. Phys.: Conf. Ser. **303**, 012105 (2011).

[19] A. Glazer and K. G. Cox, *Classical Linear Crystal Optics*, in International Tables for Crystallography Vol. D (Wiley, New York, 2006), Chap. 1.1.6.

[20] S. Seki, X. Z. Yu, S. Ishiwata, and Y. Tokura, Observation of skyrmions in a multiferroic material, Science **336**, 198 (2012).

[21] M. C. Langner, S. Roy, S. K. Mishra, J. C. T. Lee, X. W. Shi, M. A. Hossain, Y.-D. Chuang, S. Seki, Y. Tokura, S. D. Kevan, and R. W. Schoenlein, Coupled Skyrmion Sublattices in $Cu_2OSeO_3$, Phys. Rev. Lett. **112**, 167202 (2014).

[22] T. Adams, A. Chacon, M. Wagner, A. Bauer, G. Brandl, B. Pedersen, H. Berger, P. Lemmens, and C. Pfleiderer, Long-Wavelength Helimagnetic Order and Skyrmion Lattice Phase in $Cu_2OSeO_3$, Phys. Rev. Lett. **108**, 237204 (2012).

[23] E. Ruff, P. Lunkenheimer, V. V. Tsapenko, A. Loidl, H. Berger, and S. Krohns, Magnetoelectric effects in the skyrmion host material $Cu_2OSeO_3$, Sci. Rep. **5**, 15025 (2015).

[24] J.-W. G. Bos, C. V. Colin, and T. T. M. Palstra, Magnetoelectric coupling in the cubic ferrimagnet $Cu_2OSeO_3$, Phys. Rev. B **78**, 094416 (2008).

[25] O. Janson, I. Rousochatzakis, A. A. Tsirlin, M. Belesi, A. A. Leonov, U. K. Rößler, J. Van den Brink, and H. Rosner, The quantum nature of skyrmions and half-skyrmions in $Cu_2OSeO_3$, Nat. Commun. **5**, 5376 (2014).

[26] P. Y. Portnichenko, J. Romhányi, Y. A. Onykiienko, A. Henschel, M. Schmidt, A. S. Cameron, M. A. Surmach, J. A. Lim, J. T. Park, A. Schneidewind, D. L. Abernathy, H. Rosner, J. van den Brink, and D. Inosov, Magnon spectrum of the helimagnetic insulator $Cu_2OSeO_3$, Nat. Commun. **7**, 10725 (2016).

[27] M. Belesi, I. Rousochatzakis, M. Abid, U. K. Rößler, H. Berger, and J.-P. Ansermet, Magnetoelectric effects in single crystals of the cubic ferrimagnetic helimagnet $Cu_2OSeO_3$, Phys. Rev. B **85**, 224413 (2012).

[28] S. Seki, S. Ishiwata, and Y. Tokura, Magnetoelectric nature of skyrmions in a chiral magnetic insulator $Cu_2OSeO_3$, Phys. Rev. B **86**, 060403(R) (2012).

[29] M. Belesi, I. Rousochatzakis, H. C. Wu, H. Berger, I. V. Shvets, F. Mila, and J. P. Ansermet, Ferrimagnetism of the magnetoelectric compound $Cu_2OSeO_3$ probed by $^{77}Se$ NMR, Phys. Rev. B **82**, 094422 (2010).

[30] A. Aqeel, J. Baas, G. R. Blake, and T. T. M. Palstra (unpublished).

[31] K. Sato, Measurement of Magneto-optical Kerr effect using piezo-birefringent modulator, Jpn. J. Appl. Phys. **20**, 2403 (1981).

[32] S. Polisetty, J. Scheffler, S. Sahoo, Y. Wang, T. Mukherjee, X. He, and Ch. Binek, Optimization of magneto-optical Kerr setup: Analyzing experimental assemblies using Jones matrix formalism, Rev. Sci. Instrum. **79**, 055107 (2008).

[33] J. H. Yang, Z. L. Li, X. Z. Lu, M.-H. Whangbo, S.-H. Wei, X. G. Gong, and H. J. Xiang, Strong Dzyaloshinskii-Moriya Interaction and Origin of Ferroelectricity in $Cu_2OSeO_3$, Phys. Rev. Lett. **109**, 107203 (2012).

[34] R. Kuroda, S. F. Mason, T. Prosperi, S. Savage, and G. E. Tranter, Solid-state absorption and circular-dichroism spectra of five-co-ordinated trigonal copper(II) complexes: Anisotropic contributions to the *d-d* transition probabilities, J. Chem. Soc., Dalton Trans. **12**, 2565 (1981).

[35] R. Rückamp, E. Benckiser, M. W. Haverkort, H. Roth, T. Lorenz, A. Freimuth, L. Jongen, A. Möller, G. Meyer, P. Reutler, B. Büchner, A. Revcolevschi, S.-W. Cheong, C. Sekar, G. Krabbes, and M. Grüninger, Optical study of orbital excitations in transition-metal oxides, New J. Phys. **7**, 144 (2005).

[36] M. I. Aroyo, A. Kirov, C. Capillas, J. M. Perez-Mato, and H. Wondratschek, Bilbao crystallographic server. II.

Representations of crystallographic point groups and space groups, Acta Crystallogr., Sect. A: Found. Adv. **62**, 115 (2006).
[37] B. N. Figgis and M. A. Hitchman, *Ligand Field Theory and its Applications* (Wiley-VCH, Berlin, 2000).
[38] Y. P. Varshni, Temperature dependence of the energy gap in semiconductors, Physica **34**, 149 (1967).
[39] K. H. Miller, X. S. Xu, H. Berger, E. S. Knowles, D. J. Arenas, M. W. Meisel, and D. B. Tanner, Magnetodielectric coupling of infrared phonons in single-crystal $Cu_2OSeO_3$, Phys. Rev. B **82**, 144107 (2010).
[40] L. D. Barron, *Molecular Light Scattering and Optical Activity* (Cambridge University Press, New York, 2009).
[41] R. E. Newnham, *Properties of Materials: Anisotropy, Symmetry, Structure* (Oxford University Press, New York, 2008).
[42] V. S. Kurnosov, V. P. Gnezdilov, V. V. Tsapenko, P. Lemmens, and H. Berger, Analysis of the low-frequency spectrum of the cubic noncentrosymmetric ferrimagnet $Cu_2OSeO_3$, Low Temp. Phys. **38**, 489 (2012).
[43] P. S. Pershan, Magneto-optical effects, J. Appl. Phys. **38**, 1482 (1967).
[44] J.-M. Liu, *Photonic Devices* (Cambridge University Press, Cambridge, 2005).
[45] R. Chartrand, Numerical differentiation of noisy, nonsmooth data, ISRN Appl. Math. **2011**, 164564 (2011).
[46] M. Janoschek, M. Garst, A. Bauer, P. Krautscheid, R. Georgii, P. Böni, and C. Pfleiderer, Fluctuation-induced first-order phase transition in Dzyaloshinskii-Moriya helimagnets, Phys. Rev. B **87**, 134407 (2013).
[47] A. Bauer and C. Pfleiderer, in *Topological Structures in Ferroic Materials: Domain Walls, Vortices and Skyrmions* (Springer International Publishing, 2016), Chap. 1.
[48] I. Živković, J. S. White, H. M. Rønnow, K. Prša, and H. Berger, Critical scaling in the cubic helimagnet $Cu_2OSeO_3$, Phys. Rev. B **89**, 060401(R) (2014).
[49] M. Sato and Y. Ishii, Simple and approximate expressions of demagnetizing factors of uniformly magnetized rectangular rod and cylinder, J. Appl. Phys. **66**, 983 (1989).
[50] N. F. Kharchenko, A. V. Bibik, and V. V. Eremenko, Quadratic magnetic rotation of the polarization plane of light in the antiferromagnet $CoF_2$, Zh. Eksp. Teor. Fiz. **42**, 447 (1985).
[51] N. F. Kharchenko, A. V. Bibik, D. M. Desvignes, and H. Le Gall, Quadratic magnetic rotation of polarization plane of light in antiferromagnetic CaMnGe garnet, Low Temp. Phys. **20**, 296 (1994).
[52] M. Surma, Magneto-optical circular birefringence of a chiral medium in high magnetic field, Mol. Phys. **90**, 993 (1997).
[53] R. Zawodny, S. Woźniak, and G. Wagniére, On quadratic dc magnetic field-induced circular birefringence and dichroism in isotropic chiral media, Mol. Phys. **91**, 165 (1997).
[54] A. Bauer, M. Garst, and C. Pfleiderer, History dependence of the magnetic properties of single-crystal $Fe_{1-x}Co_xSi$, Phys. Rev. B **93**, 235144 (2016).
[55] Y. Okamura, F. Kagawa, S. Seki, M. Kubota, M. Kawasaki, and Y. Tokura, Microwave Magnetochiral Dichroism in the Chiral-Lattice Magnet $Cu_2OSeO_3$, Phys. Rev. Lett. **114**, 197202 (2015).
[56] R. Yasuhara, S. Tokita, J. Kawanaka, T. Kawashima, H. Kan, H. Yagi, H. Nozawa, T. Yanagitani, Y. Fujimoto, H. Yoshida, and M. Nakatsuka, Cryogenic temperature characteristics of Verdet constant on terbium gallium garnet ceramics, Opt. Express **15**, 11255 (2007).
[57] J. A. Gaj, R. R. Gałazka, and M. Nawrocki, Giant exciton Faraday rotation in $Cd_{1-x}Mn_xTe$ mixed crystals, Solid State Commun. **25**, 193 (1978).
[58] V. A. Chizhikov and V. E. Dmitrienko, Microscopic description of twisted magnet $Cu_2OSeO_3$, J. Magn. Magn. Mater. **382**, 142 (2015).
[59] R. Laiho and T. Levola, Dispersions of the optical Faraday rotation and of the refractive index in $K_2CuF_4$, Solid State Commun. **18**, 1619 (1976).
[60] H. Arend, J. Schoenes, and P. Wachter, Magneto-optical investigations of the two-dimensional ferromagnet $(CH_3NH_3)_2CuCl_4$, Phys. Status Solidi B **69**, 105 (1975).